Journal of Catalysis 359 (2018) 1–7

Contents lists available at ScienceDirect

Journal of Catalysis

journal homepage: www.elsevier.com/locate/jcat

Priority Communication

# Chemical looping epoxidation

Martin S.C. Chan [a,*], Ewa Marek [b], Stuart A. Scott [b], J.S. Dennis [a]

[a] Department of Chemical Engineering and Biotechnology, University of Cambridge, Philippa Fawcett Drive, CB3 0AS, United Kingdom
[b] Department of Engineering, University of Cambridge, Trumpington Street, CB2 1PZ, United Kingdom

ARTICLE INFO

*Article history:*
Received 10 October 2017
Revised 8 December 2017
Accepted 28 December 2017

*Keywords:*
Epoxidation
Chemical looping
Silver
Perovskite
Redox

ABSTRACT

Chemical looping epoxidation of ethylene was demonstrated, whereby the sole oxidant was a solid oxygen carrier, 15 wt% Ag supported on $SrFeO_3$. Ethylene reacted with a bed of carrier particles, without any $O_{2(g)}$ in the feed, to produce ethylene oxide (EO) and $CO_2$. Following the reduction by the $C_2H_4$ of the $SrFeO_3$, it was regenerated by passing air through the bed. The rate of reoxidation was slow, with full regeneration being achieved only by prolonged oxidation at elevated temperatures. A striking synergy between Ag and $SrFeO_3$ was observed solely when they were in intimate contact, suggesting a basis for a proposed reaction mechanism.


## 1. Introduction

Ethylene oxide (EO) is an industrially-significant chemical intermediate, with a global production of 26 million tonnes in 2013 [1]. It is used in the synthesis of polymers, antifreeze, surfactants, solvents, *etc*. The predominant technology for its production is the epoxidation of ethylene with air or purified oxygen. Silver is the only catalyst used because no other material matches its performance [2].

A key intermediate species in the reaction mechanism is the oxygen adatom ($O_a$), which is the selective oxygen species responsible for the epoxidation and, depending on its electrophilicity, combustion [3]. In the conventional process, where ethylene and gaseous oxygen are co-fed to the reactor, $O_a$ is generated from the dissociative adsorption of $O_{2(g)}$. To date, there have been no reports of $O_a$ being directly supplied from a solid oxidant, probably because of the challenging requirements imposed on such a material. Working catalysts typically operate at partial pressures of $O_2$ of up to 2 bar and temperatures of 200–300 °C [2], where evidence suggest the existence of surface silver oxide phases [4–6]. Herein, it is therefore posited that the solid oxidant needs to have a high chemical potential of oxygen, $\mu_{O2}$, to stabilise these active phases, or at least to ensure a sufficiently high surface coverage of $O_a$. Such a high $\mu_{O2}$ at these temperatures is rare among solid oxides. Sufficiently fast ionic conduction is also required to replenish $O_a$ during the reaction, but oxide ion conduction is typically slow at these temperatures. Lastly, the solid oxidant needs to be regenerable without significant loss of oxygen-storage capacity and kinetic activity.

A recent, large-scale *in silico* screening of materials has identified $SrFeO_3$ as a potential oxygen carrier for chemical looping combustion [7]. It was found that $SrFeO_3$ can release $O_{2(g)}$ reversibly over many cycles of thermal decomposition followed by reoxidation at low temperatures (~673 K, $pO_2$ = 0.15 bar), demonstrating its favourable $\mu_{O2}$ and kinetics. Crucially, $SrFeO_3$ does not react with $CO_2$ significantly [7] and thereby deactivate with the formation of carbonate, a problem afflicting other possible materials with a similar $\mu_{O2}$ such as $SrO_2$/SrO and $BaO_2$/BaO [8]. Resistance against carbonation is necessary because significant levels of $CO_2$ are generated from side reactions during epoxidation.

These favourable properties suggested the possibility of interfacing $SrFeO_3$ with Ag; $SrFeO_3$ could then supply oxygen to Ag as bulk or subsurface oxygen ($O_{ss}$), where the oxygen could then diffuse to the silver surface to be presented as $O_a$ to effect the epoxidation in the absence of $O_{2(g)}$. The concept is summarised in Fig. 1. The catalyst is then regenerated in air in a separate step to complete the chemical looping cycle.

It is advantageous to perform selective oxidations using a solid oxidant, in the absence of $O_{2(g)}$, because this avoids flammable mixtures and renders a safer process. The conversion of ethylene is no longer limited by the supply of $O_{2(g)}$, decreasing the need to recycle unreacted ethylene – industrial processes tend to operate with limited amounts of $O_2$ with ethylene in excess [2]. Furthermore, separation costs can be reduced by avoiding the need to separate $N_2$ (from purifying either $O_2$ or the products). Minimising

* Corresponding author.
*E-mail address:* mscc3@cam.ac.uk (M.S.C. Chan).

https://doi.org/10.1016/j.jcat.2017.12.030
0021-9517/

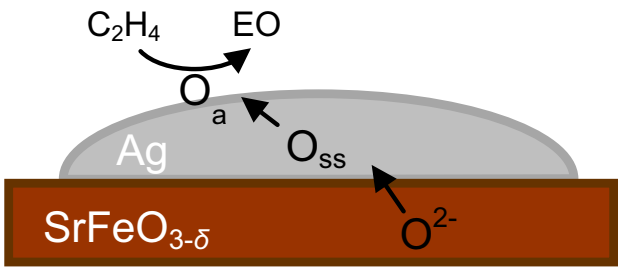


**Fig. 1.** Chemical looping epoxidation using a silver-modified oxygen carrier.

recycling, and combining unit operations of reaction and separation, are both examples of process intensification [9–11]. Lastly, improved selectivities may be achieved by the removal of $O_{2(g)}$ [12].

In this work, we show that the epoxidation may be performed in the absence of $O_{2(g)}$ by using a solid oxygen carrier. The aim is not to show competitive selectivities, so common promoters were not used (*e.g.* Cs and Cl), but rather to demonstrate the concept. We use the term 'catalyst' as an abbreviation for the 'catalyst-oxygen carrier' materials prepared in this study, where Ag acts as the catalyst and $SrFeO_3$ acts as the oxygen carrier.

## 2. Experimental methods

$SrFeO_3$ was prepared by a solid-state synthesis method. Stoichiometric amounts of $SrCO_3$ (0.72 mol) and $Fe_2O_3$ (0.36 mol) were mixed in a ball mill for 3 h at 25 Hz. Ethanol (50 mL, 99.8%, Fisher Scientific) was added as a binder to improve mixing. The mixture was dried for 24 h at 50 °C, and sieved to 180–355 μm. The particles were then calcined in four stages, with each stage consisting of calcination at 1000 °C for 3 h, followed by cooling to room temperature.

Incipient wetness impregnation was used to dose Ag onto supports, consisting of either $SrFeO_3$ or α-$Al_2O_3$. Prior to impregnation, $SrFeO_3$ was sieved to a size range of 212 – 300 μm, and α-$Al_2O_3$ (Alfa Aesar, product code 43862) was crushed and sieved to a size range of 212 – 300 μm. The volume of solution added was equal to the pore volume of the support, which was determined empirically beforehand by adding deionised water dropwise with stirring to a mass of support. The endpoint was taken to be when the granular matter just started to cohere, *i.e.* when the internal pores have been filled and the mixture is at the onset of the pendular regime, when the volume of water added was taken to be equal to the pore volume. The pore volume of $SrFeO_3$ was measured to be 0.24 mL/g, and the pore volume of α-$Al_2O_3$ was measured to be 0.26 mL/g. In a typical preparation of 15 wt% Ag/$SrFeO_3$, 1.3895 g of $AgNO_3$ (≥99.0%, Sigma-Aldrich) was dissolved in 1.2 mL water, which was then added dropwise to a batch of 5.0000 g $SrFeO_3$ with agitation by a spatula. Correspondingly, in a typical preparation of 15 wt % Ag/$Al_2O_3$, 1.3895 g of $AgNO_3$ (≥99.0%, Sigma-Aldrich) was dissolved in 1.3 mL water, which was then added dropwise to a batch of 5.0000 g $Al_2O_3$ with agitation by a spatula. The impregnated solids were then dried at 120 °C for 12 h in static air, before calcination at 500 °C for 5 h with a ramp rate of 5 °C/min in static air.

A packed bed reactor was used to perform the epoxidation experiments, and was operated in either chemical looping mode or co-feeding mode. The reactor consisted of an 8 mm i.d., 200 mm long quartz tube mounted vertically with a sintered disc fixed 75 mm from the bottom. The tube was wrapped with a high temperature dual-element heating tape (Omega, DHT052020LD). The output of the heating tape was controlled by a type K thermocouple with a mineral-insulated Inconel sheath inserted into the bed. The bed was packed above the sintered disc, with a bottom layer of α-$Al_2O_3$ (Boud Minerals, 425–710 μm) to position the active bed in the isothermal region of the reactor, then a middle layer with the catalyst, then finally another layer of 3 g of α-$Al_2O_3$ to distribute and preheat the feed. Both ends of the quartz tube were connected to Swagelok Ultra-Torr® vacuum fittings and sealed with fluorocarbon FKM O-rings. A 7 μm filter (Swagelok, SS-2TF-7) was fitted at the outlet of the reactor. *Ex situ* regeneration of the active material was performed by dismounting the reactor tube, containing the packed bed, from its fittings and placing it in a box furnace to be calcined at 400 °C for 2 h in static air.

The feed gases to the reactor were supplied from cylinders (BOC), and consisted of 5.16 vol% $C_2H_4$ in balance $N_2$ (certified to 5% uncertainty, BOC), $N_2$ (purity > 99.998%), and bottled purified air. Gas flows were manipulated by calibrated rotameters and checked using a bubble film flowmeter at the start of each experiment. Gases were switched using digitally-controlled solenoid valves. Continuous online analysis of the gaseous products was achieved by a Fourier transform infrared (FTIR) analyser (MKS Instruments, Multigas 2030) equipped with a liquid $N_2$-cooled mercury-cadmium-telluride detector. Measurements were collected 2.5 h after filling the liquid $N_2$ dewar, once the background has settled. The 5.11 m gas cell was heated to 150 °C. Each measurement consists of 8 scans of the band 800 – 4600 $cm^{-1}$, lasting 1.87 s, at a resolution of 0.5 $cm^{-1}$. The collected spectra were analysed for $C_2H_4$, $CO_2$, ethylene oxide, CO and $H_2O$, using software (MKS, MG2000). The analysis regions for each quantified species were adjusted to exclude interfering peaks from other species to eliminate any cross-sensitivities. Negligible amounts of CO were detected, <40 ppm. $H_2O$ was not quantified; its quantity was inferred from the stoichiometry of combustion, $C_2H_4 + 3/2O_2 \rightarrow CO_2 + H_2O$, *i.e.* 1 mol of $CO_2$ generated implied that 1 mol of $H_2O$ was also generated, and that 3 mol of O was consumed. No acetaldehyde was detected.

In the chemical looping experiments, the reactor was packed with 1.0 g α-$Al_2O_3$ for the bottom layer, with 2.000 g catalyst in the middle layer. A constant flow rate of 200 mL/min (measured at 293 K, 1 atm), was maintained at all times. The feed gases were switched automatically, with the base case cycling times of (i) reduction with 5.16 vol% $C_2H_4$ in balance $N_2$ for $t_{red}$ = 1.5 min, (ii) purge with $N_2$ for 2 min, (iii) oxidation with compressed air for $t_{ox}$ = 15 min, and (iv) purge with $N_2$ for 2 min.

The overall carbon balance in a particular reduction stage was calculated according to (assuming dilute gases and small conversions so that the total molar flow rate in and out of the reactor is constant)

$$\text{Carbon balance} = \frac{\text{Total carbon detected}}{\text{Total carbon fed}} = \frac{\int_{t_{start}}^{t_{end}} \left(y_{C_2H_4} + y_{EO} + \frac{1}{2}y_{CO_2} + \frac{1}{2}y_{CO}\right)dt}{y_{C_2H_4,feed} \cdot t_{red}} \quad (1)$$

where $y_i$ is the mole fraction of species $i$, $t$ is time, and $y_{C_2H_4,feed}$ is the mole fraction of $C_2H_4$ in the feed. The start and end time for integration was the first and final points in time where EO was detected (the range of this time was not necessarily equal to $t_{red}$ because of the response of the analyser). The carbon balance was always within 95 ± 5%, and usually within 98 ± 5%, which verifies that the rate of accumulation of coke in the reactor is small and may be neglected in subsequent analyses.

The cumulative amount of oxygen released by time $t$, in a particular cycle starting at time $t_{start}$, was calculated by integrating all the oxygenated gaseous products according to

$$\text{Mol O released}(t) = F\int_{t_{start}}^{t} \left(y_{EO} + 3y_{CO_2} + y_{CO}\right)dt \quad (2)$$

where $F$ is the total molar flow rate, and the term 3 $y_{CO_2}$ accounts for oxygen released from both $CO_2$ and $H_2O$ by assuming these two products are generated only from the combustion of $C_2H_4$.

In the co-feeding experiments, 2.0 g $\alpha$-$Al_2O_3$ was used for the bottom layer with 1.000 g catalyst. The flows of $C_2H_4$ and air were mixed to a composition of 4 vol% $C_2H_4$, 4 vol% $O_2$ in balance $N_2$, at a total flow rate of 200 mL/min. The instantaneous carbon balance was calculated according to

$$\text{Instantaneous carbon balance, co} - \text{feeding}(t) = \left.\frac{y_{C_2H_4} + y_{EO} + \frac{1}{2}y_{CO_2} + \frac{1}{2}y_{CO}}{y_{C_2H_4,\text{feed}}}\right|_t \quad (3)$$

The carbon balance during co-feeding was always within 97 ± 3%. The definitions of instantaneous selectivity and conversion were equivalent to those used for the chemical looping case (see Supporting Information).

The turnover frequency (TOF) for the rate of production of EO and conversion of $C_2H_4$ was calculated according to

$$\text{TOF EO} = \frac{\text{rate of production of EO}}{\text{number of surface Ag atoms}} = \frac{Fy_{EO}}{n_s m} \quad (4)$$

$$\text{TOF } C_2H_4 = \frac{\text{rate of conversion of } C_2H_4}{\text{number of surface Agatoms}} = \frac{F\left(y_{EO} + \frac{1}{2}y_{CO2}\right)}{n_s m} \quad (5)$$

where $n_s$ is the moles of surface Ag atoms per unit mass of catalyst and $m$ is the mass of catalyst. The approximation that the rate of reaction = $Fy_i$ was used because the change in the total molar flow of gas can be neglected for dilute feeds with small conversion.

Brunauer, Emmett and Teller (BET) theory [13] was used to model nitrogen physisorption isotherms measured at 77 K (Tristar 3000, Micromeritics). 1–2 g of the supported silver samples were used in each analysis.

Thermogravimetric analysis (TGA) was conducted using a TGA/DSC1 (Mettler Toledo). Approximately 20 mg of 15 wt% Ag/$SrFeO_3$ was loaded into a 70 μL alumina crucible. The sample was heated to 270 °C in air. 5 min after reaching the setpoint temperature, the gas was switched to $N_2$ for 2 min to purge. Ethylene was then fed to the sample for 30 min, followed by a 2 min purge with $N_2$, then air was fed for 60 min. Throughout the experiments, the TGA chamber was purged with protective and purge gas flows of Ar (50 mL/min each, measured at 293 K and 1 atm). The reactive gas was supplied through a capillary tube located above the crucible at 50 mL/min (measured at 293 K and 1 atm). The reactive gases fed from cylinders were air, $N_2$, 5.16% $C_2H_4$ in balance $N_2$ (all BOC, >99.99%). The actual concentrations of the specific gas components listed above were approximately three times lower when in contact with the solid sample due to the dilution with the protective and purge gas.

Scanning electron microscopy (SEM) images were taken using a Leo GEMINI 1530 VP. The particulate samples of 15 wt% Ag/$SrFeO_3$ were mounted on copper tape. Images were taken at an accelerating voltage of 2.4 kV and a working distance of 5.4 – 5.6 mm. Distributions of particle size were measured from the SEM images with ImageJ [14]. The analysis was carried out semi-automatically, using the 'Analyze Particles' function in ImageJ. The results were then inspected manually to correct for any false measurements, *e.g.* aggregated particles. Each analysed particle $i$ was described by its projected area $A_i$, from which an equivalent diameter may be calculated $d_i = 2\sqrt{A_i/\pi}$. The surface area-weighted mean diameter was then calculated using $d_{3,2} = \frac{\sum d_i^3}{\sum d_i^2}$, which was taken to be the mean crystallite size. 458 particles were measured for Ag/$SrFeO_3$, and 83 particles for Ag/$Al_2O_3$. The dispersion of silver, $D$, was calculated by assuming spherical particles, so

$$D = \frac{\text{number of surface Ag atoms}}{\text{total number of Ag atoms}} = \frac{\rho_s \times \pi d_{3,2}^2}{\rho_b \times \frac{\pi d_{3,2}^3}{6}} = \frac{6\rho_s}{\rho_b}\frac{1}{d_{3,2}} = \frac{6 \times 1.14 \times 10^{19}}{5.87 \times 10^{28}}\frac{1}{d_{3,2}[\text{m}]} = \frac{1.17}{d_{3,2}[\text{nm}]} \quad (6)$$

where $\rho_s = 1.14 \times 10^{19}$ $m^{-2}$ is the surface atom density of silver averaged over the (1 0 0), (1 1 0) and (1 1 1) planes, and $\rho_b = 5.87 \times 10^{28}$ $m^{-3}$is the bulk atom density of silver (fcc lattice parameter is 0.40853 nm). The moles of surface Ag atoms per unit mass of catalyst, $n_s$, can then be calculated from the loading of silver using $n_s = Dw/m_{Ag}$ where $w = 15$ wt % is the loading of Ag on the catalyst and $m_{Ag} = 108$ g $mol^{-1}$ is its molecular weight.

Power X-ray diffraction was performed on the supported silver samples using Cu-Kα radiation with a voltage of 40 kV and current 40 mA (Empyrean, PANalytical). The diffractogram was collected in the range of 2θ from 10° to 150° over 67 min. The mean particle size of the silver crystallites was measured by Rietveld refinement of the diffraction patterns. The refined parameters were particle size, strain, unit cell and atomic displacement. The surface area-weighted mean diameter was calculated using the method reported by Popa and Balzar (2002) [15]. The lack of measurable peak-broadening in the $Al_2O_3$-supported sample suggested that the particles were at least 300 nm. Nevertheless, measurements for both $Al_2O_3$- and $SrFeO_3$-supported samples were consistent with SEM imaging. The refined XRD pattern for Ag/$SrFeO_3$ can be found in the Supporting Information.

## 3. Results

The catalyst, composed of 15 wt% Ag supported on $SrFeO_3$, was evaluated in a packed bed reactor (*n.b* here, the nonstoichiometric perovskite $SrFeO_{3-\delta}$ is abbreviated as $SrFeO_3$ for brevity, its characterisation was reported by Lau et al., (2017) [7]). A typical experiment is shown in Fig. 2, which shows how the mole fractions varied over 10 cycles. Within each cycle, air is first fed to the reactor (indicated by the background level of ~440 ppm $CO_2$ in the cylinder of compressed air) to charge the catalyst with oxygen, followed by a purge with $N_2$, then a switch to a feed of ethylene to produce EO and $CO_2$, followed by another purge. The selectivity and conversion achieved by the catalyst decayed gradually with cycling, before approaching an asymptote. This decay is probably caused by the slow rate of reoxidation of the perovskite. Thermogravimetric analysis, presented in Fig. 3, shows that the rate of oxidation in air was indeed much slower than the rate of reduction in ethylene. This is supported by the results in Fig. 4, which show the effect of varying the duration of reduction and oxidation. When the duration of oxidation was increased from $t_{ox}$ = 7.5 min to 30 min, both the selectivity and conversion were maintained at higher values. A similar improvement was observed when the duration of reduction was decreased from $t_{red}$ = 3 min to 1 min. The decrease in conversion is probably caused by the depletion of oxygen species, owing to the catalyst gradually becoming more reduced with cycling. Cycling with 5 min reduction and 10 min oxidation (data not shown) led to the mole fraction of EO decaying to zero within four cycles. Accumulation of coke, indicated by slight elevations in the mole fraction of $CO_2$ (of the order of 10 ppm) during oxidation with air, may also have caused the decaying activity. The decrease in selectivity might be explained by the depletion of subsurface oxygen species, $O_{ss}$, when the catalyst was reduced. The decrease in abundance of $O_{ss}$ would cause the degree of electrophilicity of $O_a$ to decrease [16,17], resulting in the observed decrease in selectivity.

The regenerability of the 15 wt% Ag/$SrFeO_3$ catalyst was examined further by calcining the cycled sample *ex situ* in static air at

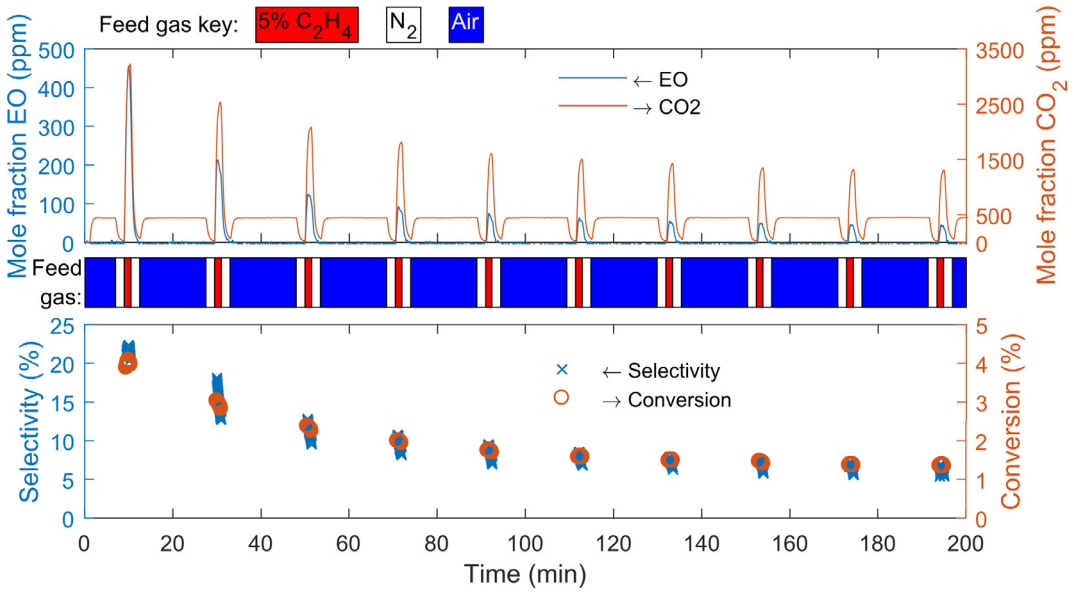


**Fig. 2.** Mole fraction, selectivity and conversion profiles from a packed bed reactor operated in chemical looping mode, using 15 wt% Ag/$SrFeO_3$ as the catalyst. The background of $CO_2$ during oxidation steps was from compressed atmospheric air. Conditions: 270 °C, 1 atm, 2.000 g catalyst, gas feed of 200 mL/min (as measured at 293 K, 1 atm). Cycling times: (i) $t_{red}$ = 1.5 min reduction with 5.16 vol% $C_2H_4$ in balance $N_2$, (ii) 2 min purge with $N_2$, (iii) $t_{ox}$ = 15 min oxidation with air, (iv) 2 min purge with $N_2$.

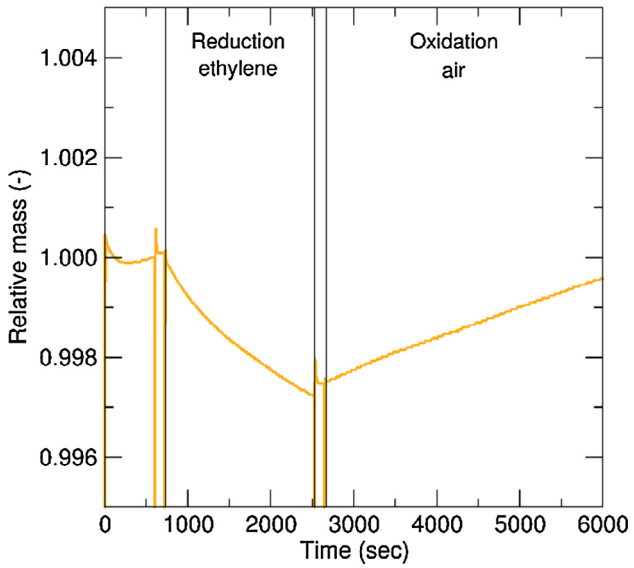


**Fig. 3.** Variation of catalyst mass over a single cycle for a sample of 15 wt% Ag/$SrFeO_3$ measured by TGA. The temperature was fixed at 270 °C. The spikes in the mass are artefacts caused by the switching of gases.

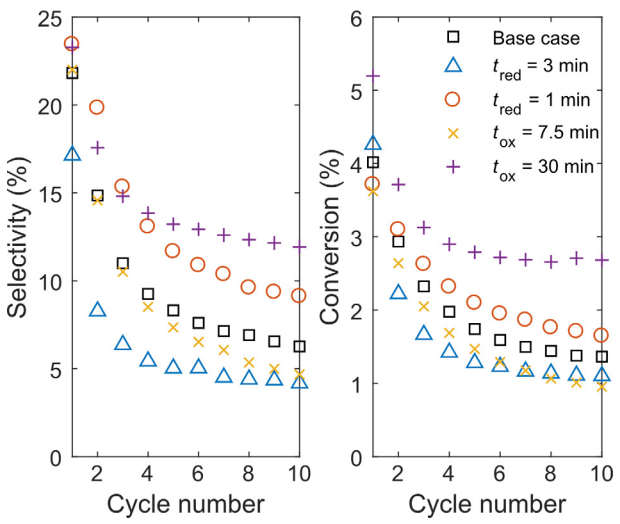


**Fig. 4.** Effects of cycling times on the selectivity and conversion. Conditions: 270 °C, 1 atm, 2.000 g of 15 wt% Ag/$SrFeO_3$, feed of 200 mL/min (as measured at 293 K, 1 atm). Cycling times (unless stated otherwise): (i) $t_{red}$ = 1.5 min reduction with 5.16 vol% $C_2H_4$ in balance $N_2$, (ii) 2 min purge with $N_2$, (iii) $t_{ox}$ = 15 min oxidation with air, (iv) 2 min purge with $N_2$.

400 °C for 2 h, before subjecting it to the same ten cycles. This was repeated three times, shown in Fig. 5. It can be seen that this treatment fully regenerated both the selectivity and activity of the catalyst, confirming that the oxidation step is probably the rate-limiting step in the cycle. Additionally, coke should have been effectively removed by this period of oxidation. Fig. 5 also shows that the selectivity gradually improved over time, which might be related to the sintering of the Ag particles. The selectivity of Ag particles, for epoxidation, increases with their size [18,19]. Scanning electron microscopy (SEM) images of the fresh and cycled catalysts, presented in Fig. 6, show that Ag particles as small as 50 nm present on the fresh catalyst were no longer present on the cycled catalyst.

Generally, over the course of one cycle, the instantaneous selectivity of the carrier decreased as it became more reduced. This is shown in Fig. 7 for the sample which has been regenerated thrice at 400 °C for 2 h (*i.e.* cycles 31–40 in Fig. 5). The trend is consistent with the mechanism proposed earlier, that reduction of the catalyst led to a gradual depletion of $O_a$ and $O_{ss}$, resulting in the decreasing selectivity. Interestingly, the first cycle after each calcination step always exhibited a maximum in selectivity and conversion (*n.b.* the early maxima for subsequent cycles are probably artefacts of the response time of the gas analyser, or noise). This gradual improvement in the selectivity during the first cycle in Fig. 7 might be due to carbon deposition which selectively poisoned unselective sites [20].

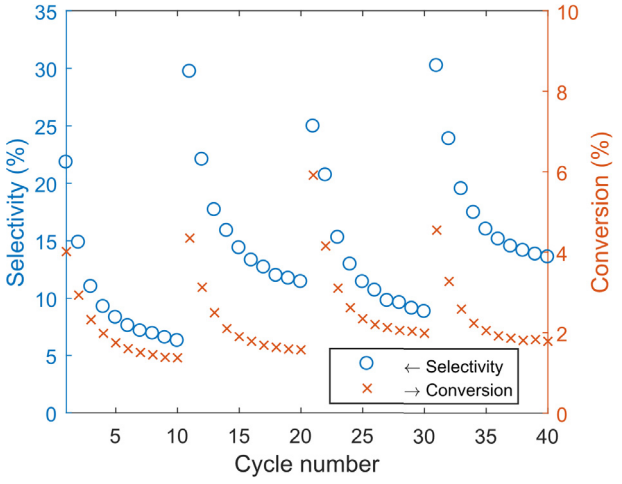


**Fig. 5.** Effect of extended *ex-situ* reoxidation at 400 °C for 2 h, performed after every 10th cycle. Conditions: 270 °C, 1 atm, 2.000 g of 15 wt% Ag/$SrFeO_3$, feed of 200 mL/min (as measured at 293 K, 1 atm). Cycling times: (i) $t_{red}$ = 1.5 min reduction with 5.16 vol% $C_2H_4$ in balance $N_2$, (ii) 2 min purge with $N_2$, (iii) $t_{ox}$ = 15 min oxidation with air, (iv) 2 min purge with $N_2$.

## 4. Discussion

The performance of Ag/$SrFeO_3$ was in stark contrast with those of (i) 15 wt% Ag/$Al_2O_3$ and (ii) a heterogeneous mixture of particles of 15 wt% Ag/$Al_2O_3$ with particles of $SrFeO_3$, shown in Fig. 8. The 15 wt% Ag/$Al_2O_3$ catalyst yielded only barely detectable levels of EO (~10 ppm) with instantaneous selectivities of up to ~30% in the first cycle, and no detectable EO in subsequent cycles. The production of $CO_2$ also quickly fell to insignificant levels (<30 ppm). This is because neither Ag nor $Al_2O_3$ can carry enough oxygen over from the preceding oxidation step in the cycle, so the subsequent reaction with ethylene became starved of oxygen. With the addition of separate particles of $SrFeO_3$ to the bed, only $CO_2$ was produced. This is because the perovskite could not generate $O_a$ by itself nor did it supply any oxygen to Ag/$Al_2O_3$, which prevented epoxidation from occurring and so only combustion occurred. This also shows that some $CO_2$ evolved in the reaction with Ag/$SrFeO_3$ must have originated from reaction with the part of the $SrFeO_3$ surface not covered with Ag. Therefore, the selectivity could be improved simply by increasing the coverage of $SrFeO_3$ with Ag. The experiment with bare $SrFeO_3$ also eliminates the possibility of $SrFeO_3$ supplying oxygen to Ag *via* gaseous transport at this temperature. Hence, the performance of 15 wt% Ag/$SrFeO_3$ must have originated from the intimate physical contact between Ag and $SrFeO_3$, suggesting possible mechanisms: (i) solid state oxygen diffused from $SrFeO_3$ to Ag, as hypothesised, (ii) the oxygen storage capacity of Ag became enhanced, or (iii) Ag facilitated adsorption and diffusion of ethylene to the $SrFeO_3$ boundary to react with lattice oxygen from $SrFeO_3$, *i.e.* triple phase boundaries. However, because of the magnitude of the effect, the mechanism of (ii) seems unlikely; if one assumes that all the oxygen in the products originated solely from Ag, then the bulk chemical state of the silver phase would be written as $AgO_{0.08}$ (for the first cycle with $t_{red}$ = 3 min), which is far higher than the limit of solubility (O:Ag molar ratio ~$10^{-6}$) [21]. Moreover, bulk silver oxide is not thermodynamically stable at these conditions [21]. Adsorbed oxygen also cannot account for the capacity because the amount of oxygen released exceeded the number of surface Ag sites. As shown in Table 1, the molar ratio of O released to surface Ag = 7.7 exceeded an adsorption stoichiometry of 1, which is generally assumed for chemisorption analyses [22]. Furthermore, adsorbed oxygen should also be accessible by Ag/$Al_2O_3$ and yet it did not exhibit much activity, probably because oxygen desorbed from Ag during the $N_2$ purge, which would be significant at these temperatures [23]. Triple phase boundaries producing $CO_2$ through the mechanism of (iii) cannot yet be excluded, but the formation of ethylene oxide through this mechanism is unlikely because epoxidation proceeds from the formation of oxametallacycles [24]. In conclusion, $SrFeO_3$ most likely donated oxygen to Ag to be presented as adatoms on the Ag surface through the mechanism of (i). This might well be exploitable in catalyst-oxygen carrier systems other than Ag-$SrFeO_3$ shown herein and applicable to selective oxidations other than the epoxidation of ethylene.

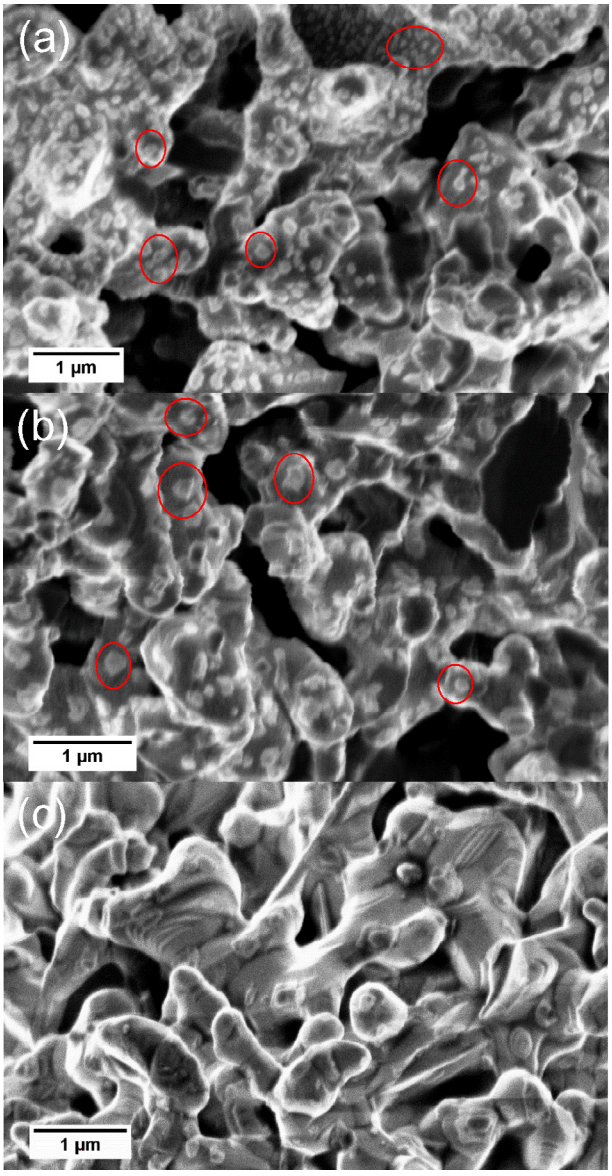


**Fig. 6.** SEM images of 15 wt% Ag/$SrFeO_3$ (a) initial state after first calcination at 500 °C for 5 h, (b) cycled and regenerated multiple times, and (c) bare $SrFeO_3$. Ag crystallites as small as 50 nm are present in (a), whereas only crystallites > 100 nm appear in (b). Selected individual and clusters of crystallites have been circled in red for clarity.

The Ag/$Al_2O_3$ and Ag/$SrFeO_3$ catalysts were also examined in a co-feeding mode, using gas-phase oxygen, where the feed was a premixed stream of $O_2$ (4 vol%) and $C_2H_4$ (4 vol%), with 200 mL/min total flow (as measured at 293 K and 1 atm) and 1.000 g catalyst (half the catalyst loading compared to the chemical looping experiments). After 5 h on stream, Ag/$Al_2O_3$ achieved a conversion

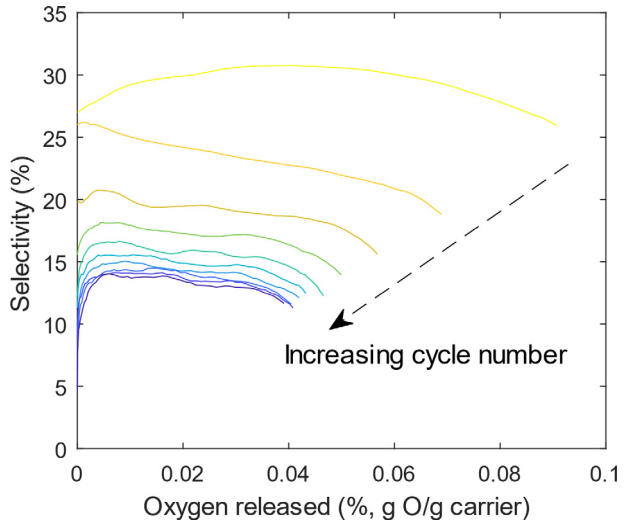


**Fig. 7.** Variation of instantaneous selectivity with degree of reduction of catalyst, expressed as the total amount of oxygen released. Each line corresponds to one cycle. Conditions: 270 °C, 1 atm, 2.000 g of 15 wt% Ag/$SrFeO_3$, feed of 200 mL/min (as measured at 293 K, 1 atm). Cycling times: (i) $t_{red}$ = 1.5 min reduction with 5.16 vol% $C_2H_4$ in balance $N_2$, (ii) 2 min purge with $N_2$, (iii) $t_{ox}$ = 15 min oxidation with air, (iv) 2 min purge with $N_2$.

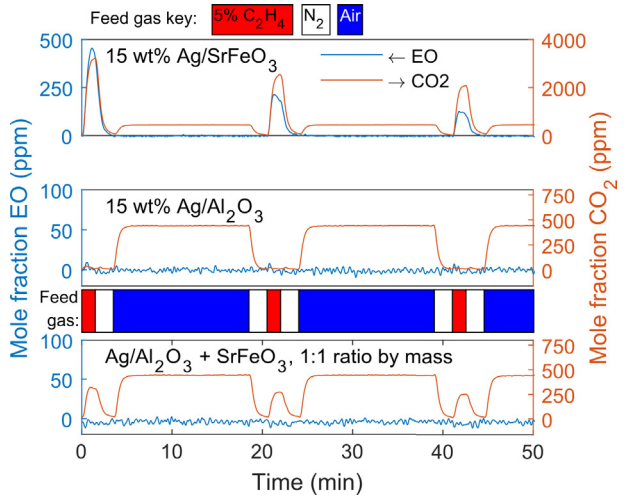


**Fig. 8.** Effect of the support on the performance in chemical looping mode. Conditions: 270 °C, 1 atm, 2.000 g of catalyst, feed of 200 mL/min (as measured at 293 K, 1 atm). Cycling times: (i) $t_{red}$ = 1.5 min reduction with 5.16 vol% $C_2H_4$ in balance $N_2$, (ii) 2 min purge with $N_2$, (iii) $t_{ox}$ = 15 min oxidation with air, (iv) 2 min purge with $N_2$.

of 1.6% at a selectivity of 27%, whilst Ag/$SrFeO_3$ achieved a conversion of 6% at a selectivity of 5.7%. Turnover frequencies (TOF) from these co-feeding experiments are shown in Table 1. TOFs were also calculated for the Ag/$SrFeO_3$ sample in chemical looping mode, shown in Fig. 9. Whilst the TOF apparently increased up to ~0.03 wt% of oxygen released, this is probably an artefact caused by the response time of the analyser. It is feasible for the TOF to have linearly decayed right from the start, which is typical for certain types of gas-solid reactions, and that convolution with the analyser masked this initial period. TOF then decayed from maxima of $1.1 \times 10^{-2}$ $C_2H_4$ $s^{-1}$ and $0.24 \times 10^{-2}$ EO $s^{-1}$, because the amount of oxygen depleted. The observed TOFs in this study were within the generally-observed range of $10^{-3}$–$10^{-1}$ $s^{-1}$ for unpromoted supported polycrystalline Ag catalysts [22,25]. It is not surprising that the chemical looping TOF was on the lower end of this range, because the lattice oxygen from $SrFeO_3$ has additional resistances for transport to the Ag active sites compared to gaseous oxygen.

Whilst the selectivities and TOFs shown in the chemical looping experiments were worse than those of the conventional co-feeding experiments, they were within an order of magnitude and we note that there are many degrees of freedom available to optimise the performance of both, or separately, the catalyst and the oxygen carrier, in addition to the operating parameters. No such optimisation was undertaken in producing these results, but will be explored in a future study. It is noteworthy that the instantaneous

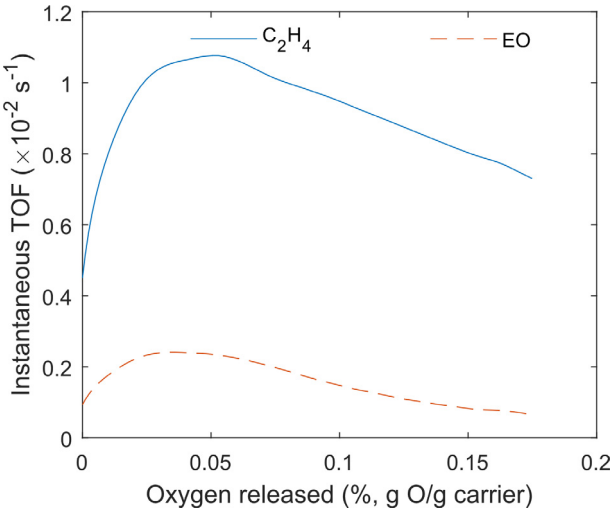


**Fig. 9.** Turnover frequencies, based on the rates of $C_2H_4$ conversion and EO production, varying with the degree of reduction during the first cycle. Conditions: 270 °C, 1 atm, 2.000 g of 15 wt% Ag/$SrFeO_3$, feed of 200 mL/min (as measured at 293 K, 1 atm). Reduction in 5.16 vol% $C_2H_4$ over a period of 3 min.

**Table 1**
Characterisation and turnover frequencies (TOF), based on $C_2H_4$ conversion or EO production, of the prepared catalysts.

| Sample | BET surface area | Mean particle size XRD | Mean particle size SEM | Silver dispersion SEM | Ag surface area | Moles of surface Ag | Chemical looping[a] | | | | Co-feeding | |
|---|---|---|---|---|---|---|---|---|---|---|---|---|
| | | | | | | | Oxygen released | $\frac{O\ released}{Surface\ Ag}$ | TOF $C_2H_4$ | TOF EO | TOF $C_2H_4$ | TOF EO |
| | $m^2\ g^{-1}$ | nm | nm | – | $m^2\ g^{-1}$ | mol Ag $g^{-1}$ | mol O $g^{-1}$ | – | $\times 10^{-2}\ s^{-1}$ | $\times 10^{-2}\ s^{-1}$ | $\times 10^{-2}\ s^{-1}$ | $\times 10^{-2}\ s^{-1}$ |
| 15 wt% Ag/$SrFeO_3$ | 0.92 | 110 ± 40 | 107 ± 3 | $1.09 \times 10^{-2}$ | 0.80 | $1.5 \times 10^{-5}$ | $1.2 \times 10^{-4}$ [b] | 7.7 [b] | 1.1 [b] | 0.24 [b] | 2.2 | 0.13 |
| 15 wt% Ag/$Al_2O_3$ | 0.22 | >300 | 2740 ± 80 | $4.27 \times 10^{-4}$ | 0.031 | $5.9 \times 10^{-7}$ | | | | | 15 | 4.3 |

[a] First cycle with reduction time $t_{red}$ = 3 min. Maximum instantaneous values for TOF.
[b] No detected activity.

performance near the start of chemical looping operation briefly surpassed the co-feeding operation, and that this could be reliably reproduced with a long regenerating treatment at elevated temperatures in air – we speculate that tuning the material properties for faster reoxidation to sustain this early transient will be particularly important.

## 5. Conclusions

The epoxidation of ethylene in the absence of gaseous oxygen depended crucially upon the intimate contact between the catalyst, Ag, and the oxygen carrier, $SrFeO_3$. This intimate contact suggests that solid state transport of oxygen from $SrFeO_3$ to Ag was responsible for the observed performance, but further study is needed to confirm this mechanism. Effects of the operation conditions were studied, which showed that the oxidation step in the cycle is probably the bottleneck, being slower than the reduction step, and that further attention on this part of the process is crucial. Comparable, although currently inferior, performance with conventional co-feeding justifies further development of this technology.

## Acknowledgements

MSCC acknowledges funding from an ESPRC Doctoral Training Grant, and from an IChemE Andrew Fellowship. The research was carried out with the financial support from EPSRC grant no. EP/K030132/1. Maxime Duvieusart and Brian Graves are acknowledged for help with the SEM images. Dr Robert B Grant is acknowledged for help with the FTIR and for helpful discussions on the epoxidation mechanism. Dr Michael W Gaultois is acknowledged for the XRD Rietveld analysis. Zlatko Saracevic is acknowledged for help with the nitrogen adsorption analysis.

## Appendix A. Supplementary material

XRD pattern of 15 wt% Ag/$SrFeO_3$. Deconvolution of mole fractions from analyser response. Definitions of selectivity and conversion. Open data access available from https://www.repository.cam.ac.uk. Supplementary data associated with this article can be found, in the online version, at https://doi.org/10.1016/j.jcat.2017.12.030.

## References

[1] C.H. McAteer, R. Murugan, Y. V. Subba Rao, Heterogeneously Catalyzed Synthesis of Heterocyclic Compounds, in: Adv. Heterocycl. Chem., Elsevier Ltd, 2017: pp. 173–205. doi:10.1016/bs.aihch.2016.03.003.
[2] S. Rebsdat, D. Mayer, Ethylene Oxide, Ullmann's Encycl. Ind. Chem. (2012) 547–572. doi:10.1002/14356007.a10_117.
[3] R.M. Lambert, F.J. Williams, R.L. Cropley, A. Palermo, Heterogeneous alkene epoxidation: past, present and future, J. Mol. Catal. A Chem. 228 (2005) 27–33, https://doi.org/10.1016/j.molcata.2004.09.077.
[4] A. Michaelides, M.L. Bocquet, P. Sautet, A. Alavi, D.A. King, Structures and thermodynamic phase transitions for oxygen and silver oxide phases on Ag{1 1 1}, Chem. Phys. Lett. 367 (2003) 344–350, https://doi.org/10.1016/S0009-2614(02)01699-8.
[5] S. Piccinin, S. Zafeiratos, C. Stampfl, T.W. Hansen, M. Hävecker, D. Teschner, V.I. Bukhtiyarov, F. Girgsdies, A. Knop-Gericke, R. Schlögl, M. Scheffler, Alloy catalyst in a reactive environment: the example of Ag-Cu particles for ethylene epoxidation, Phys. Rev. Lett. 104 (2010) 1–4, https://doi.org/10.1103/PhysRevLett. 104.035503.
[6] R. Reichelt, S. Günther, M. Rößler, J. Wintterlin, B. Kubias, B. Jakobi, R. Schlögl, High-pressure STM of the interaction of oxygen with Ag(1 1 1), Phys. Chem. Chem. Phys. 9 (2007) 3590–3599, https://doi.org/10.1039/B700432J.
[7] C.Y. Lau, M.T. Dunstan, W. Hu, C.P. Grey, S.A. Scott, Large scale in silico screening of materials for carbon capture through chemical looping, Energy Environ. Sci. 10 (2017) 818–831, https://doi.org/10.1039/C6EE02763F.
[8] W.B. Jensen, The origin of the brin process for the manufacture of oxygen, J. Chem. Educ. 86 (2009) 1266, https://doi.org/10.1021/ed086p1266.
[9] J.-C. Charpentier, In the frame of globalization and sustainability, process intensification, a path to the future of chemical and process engineering (molecules into money), Chem. Eng. J. 134 (2007) 84–92, https://doi.org/10.1016/j.cej.2007.03.084.
[10] T. Van Gerven, A. Stankiewicz, Structure, energy, synergy, time - the fundamentals of process intensification, Ind. Eng. Chem. Res. 48 (2009) 2465–2474, https://doi.org/10.1021/ie801501y.
[11] Y. Kim, L.K. Park, S. Yiacoumi, C. Tsouris, Modular chemical process intensification: a review, Annu. Rev. Chem. Biomol. Eng. 8 (2017) 359–380, https://doi.org/10.1146/annurev-chembioeng-060816-101354.
[12] S. Yusuf, L.M. Neal, F. Li, Effect of promoters on manganese-containing mixed metal oxides for oxidative dehydrogenation of ethane via a cyclic redox scheme, ACS Catal. 7 (2017) 5163–5173, https://doi.org/10.1021/acscatal.7b02004.
[13] S. Brunauer, P.H. Emmett, E. Teller, Adsorption of gases in multimolecular layers, J. Am. Chem. Soc. 60 (1938) 309–319, https://doi.org/10.1021/ja01269a023.
[14] C.A. Schneider, W.S. Rasband, K.W. Eliceiri, NIH Image to ImageJ: 25 years of image analysis, Nat. Methods. 9 (2012) 671–675, https://doi.org/10.1038/nmeth.2089.
[15] N.C. Popa, D. Balzar, An analytical approximation for a size-broadened profile given by the lognormal and gamma distributions, J. Appl. Crystallogr. 35 (2002) 338–346, https://doi.org/10.1107/S0021889802004156.
[16] M.O. Özbek, R.A. van Santen, The mechanism of ethylene epoxidation catalysis, Catal. Letters. 143 (2013) 131–141, https://doi.org/10.1007/s10562-012-0957-3.
[17] M.C.N. Amorim de Carvalho, F.B. Passos, M. Schmal, Study of the active phase of silver catalysts for ethylene epoxidation, J. Catal. 248 (2007) 124–129, https://doi.org/10.1016/j.jcat.2006.10.030.
[18] V.I. Bukhtiyarov, A. Knop-Gericke, Ethylene Epoxidation Over Silver Catalysts, in: C. Hess, R. Schlögl (Eds.), Nanostructured Catal. Sel. Oxid., Royal Society of Chemistry, Cambridge, 2011: pp. 214–247. doi:10.1039/9781847559876.
[19] P. Christopher, S. Linic, Shape- and size-specific chemistry of ag nanostructures in catalytic ethylene epoxidation, ChemCatChem. 2 (2010) 78–83, https://doi.org/10.1002/cctc.200900231.
[20] C.H. Collett, J. McGregor, Things go better with coke: the beneficial role of carbonaceous deposits in heterogeneous catalysis, Catal. Sci. Technol. 6 (2016) 363–378, https://doi.org/10.1039/C5CY01236H.
[21] J. Assal, B. Hallstedt, L.J. Gauckler, Thermodynamic assessment of the silver-oxygen system, J. Am. Ceram. Soc. 80 (1997) 3054–3060, https://doi.org/10.1111/j.1151-2916.1997.tb03232.x.
[22] J. Lu, J.J. Bravo-Suárez, A. Takahashi, M. Haruta, S.T. Oyama, In situ UV-vis studies of the effect of particle size on the epoxidation of ethylene and propylene on supported silver catalysts with molecular oxygen, J. Catal. 232 (2005) 85–95, https://doi.org/10.1016/j.jcat.2005.02.013.
[23] G.W. Busser, O. Hinrichsen, M. Muhler, The temperature-programmed desorption of oxygen from an alumina-supported silver catalyst, Catal. Letters. 79 (2002) 49–54, https://doi.org/10.1023/A:1015300520227.
[24] S. Linic, H. Piao, K. Adib, M.A. Barteau, Ethylene epoxidation on Ag: identification of the crucial surface intermediate by experimental and theoretical investigation of its electronic structure, Angew. Chemie Int. Ed. 43 (2004) 2918–2921, https://doi.org/10.1002/anie.200353584.
[25] S.R. Seyedmonir, J.K. Plischke, M.A. Vannice, H.W. Young, Ethylene oxidation over small silver crystallites, J. Catal. 123 (1990) 534–549, https://doi.org/10.1016/0021-9517(90)90149-E.